*Progress In Electromagnetics Research M, Vol. 41, 95–104, 2015*

# Resolution Enhancement for LASAR 3D Imaging via $\ell_1$ Regularization and SVA

**Gao Xiang*, Xiaoling Zhang, Jun Shi, and Shunjun Wei**

**Abstract**—Linear array SAR (LASAR) has been attracting more and more attention for its capability of obtaining three dimensional (3D) resolutions. However, the low resolution in cross track (CT) direction limited by the length of its linear antenna array has become the bottleneck of its practical applications. To overcome this problem, we present a novel algorithm based on sparse reconstruction (SR) to improve the resolution in CT direction. First, it establishes a 1D real-valued sparse model for LASAR, which deals with the 3D image column by column along CT direction in each equi-range slice. This enables it to handle large scenes. Second, it employs the spatially variant apodization (SVA) to filter bases of the measurement matrix. As a result, the cross coherence gets suppressed as well, and it is helpful to improve the performance of sparse reconstruction algorithms (SRAs). Third, we propose the resolution enhancement ability (REA), which provides a new idea to evaluate how many times the resolution could be improved. Experimental results validate that when the signal to noise ratio (SNR) is 30 dB, LASAR could usually obtain 2 times of resolution improvement in CT direction, while the proposed method further improves the REA by a factor about 2.5. Moreover, the 3D surface terrain simulation shows a great improvement for the digital elevation map (DEM) in resolution enhancement.

## 1. INTRODUCTION

Three-dimensional (3D) SAR imaging has been attracting more and more researchers' attention over the recent years, since it has broad application prospects [1], such as safe navigation, terrain mapping, and disaster monitoring. As known to all, there are mainly three types of 3D SAR imaging system, namely, Interferometric SAR (InSAR) [2, 3], LASAR [4] and Circular/Curvilinear SAR (CSAR) [5–7]. Compared with InSAR, LASAR and CSAR are usually considered to obtain true 3D spatial resolutions of a scatter, while InSAR obtains only a height of the 2D resolution cell, such that it cannot distinguish two scatters in the same 2D resolution cell in elevation direction. Besides, LASAR has a better peak sidelobe ratio (PSLR) and easier flight path controlling than CSAR [8]. Thus, LASAR is more promising practical application, and we are concerned about LASAR in our paper.

LASAR was first proposed by Mahafza and Sajjadi in [4]. From 2005 to 2006, the FGAN of Germany developed the Airborne Radar for Three-dimensional Imaging and Nadir Observation (ARTINO) system, which employed phase center approximation (PCA) and multiple input multiple output (MIMO) concepts to reduce the system costs [1, 9]. In 2009, Shi et al. reported some experimental results of the *One-active LASAR* system [10]. Besides, LASAR can also be extended to forward-looking model [11, 12]. However, the low resolution in CT direction, which is limited by the length of the physical linear array, becomes the bottleneck of practical applications of LASAR. Therefore, it is necessary to develop effective resolution enhancement (RE) algorithms for LASAR.

*Received 19 December 2014, Accepted 13 February 2015, Scheduled 21 February 2015*
* Corresponding author: Gao Xiang (moran422@gmail.com).
The authors are with the University of Electronic Science and Technology of China (UESTC), Chengdu, P. R. China.

To improve the resolution of SAR image, there have been many methods based on spectral estimation and spectrum extrapolation. López-Dekker et al. have proposed to focus the SAR image by spectral estimation algorithms Capon and Amplitude and Phase Estimation (APES) in [13]. They found that the Capon- and APES- based methods could improve resolutions and reduce sidelobes of SAR image. Xu and Narayanan have researched an iterative method based on super-SVA for SAR resolution improvement [14]. And it could usually improve the resolution by about 2 times. Lim et al. have presented a non-iterative super-resolution technique combining super-SVA with modified geometric mean filter [15]. It could avoid iterative calculations to save computational complexity and improve the resolution by about 40%.

In recent decades, sparse reconstruction (SR) has been greatly developed and applied to many fields [16, 17]. Because 3D imaging needs only to recovery the surface of an object, its images are usually sparse in 3D imaging space. This property encourages researchers to apply SR to 3D imaging. In [17], Potter et al. introduced that compressive sensing (CS) could be used to enhance the CSAR image. In [18], Zhu and Bamler researched the resolution enhancement problem for Tomographic SAR in elevation direction with CS methods. It aimed to resolve two closely spaced complex-valued points from a certain number of measurements. LASAR is different from Tomographic SAR that LASAR has lower resolution in CT direction and might have more than two scatters to be recovered. For LASAR, Wei and Zhang [19] and Shi et al. [20] presented CS based frameworks for 3D SAR imaging by handling the problem slice by slice in elevation direction. However, they are still storage consuming and not suitable for large slice images. In [21], Wei and Zhang proposed a 1D complex-valued CS based algorithm to focus the data of CT direction. It reduced the size of measurement matrix and obtained enhanced 3D images. However, [19–21] mainly address how to apply CS to LASAR imaging, but do not focus on *resolution enhancement*. In this paper, we concentrate on the RE of LASAR. There are two main contributions: (1) It proposes a novel resolution enhancement algorithm based on a 1D real-valued sparse model of LASAR, which employs SVA [22] to filter bases of the measurement matrix. This model is suitable for large problems and promising to have better performance in RE; (2) It presents the resolution enhancement ability (REA) parameter to evaluate how many times the resolution could be improved by SRAs. It could provide a proper pixel interval (resolution) for the sparse recovery image.

The remaining sections of this paper are organized as follows. In Section 2, we present a 1D real-valued sparse model for LASAR, then the pixel interval and cross coherence of the measurement matrix are analyzed in detail. In Section 3, for a better performance in RE, we suggest to filter bases of the measurement matrix by SVA [22]. In Section 4, we propose the REA of LASAR and examine the proposed method by Monte Carlo experiments and a 3D surface terrain simulation.

## 2. RESOLUTION ENHANCEMENT FRAMEWORK

In this section, we first introduce the geometrical model of LASAR briefly. Then a 1D sparse model of LASAR, which concentrates on the resolution enhancement in CT direction, is established. Finally, the pixel interval and cross coherence of the measurement matrix are analyzed in detail.

### 2.1. 1D Sparse Model of LASAR

Though LASAR usually uses a sparse MIMO array to transmit and receive signals, it can always be interpreted as a uniform linear array (ULA) contributed to the PCA principle. Thus, without loss of generality, we assume the LASAR mounts a ULA directly in this paper, as shown in Figure 1. Where $x$-axis, $y$-axis and $z$-axis denote the along-track (AT) direction, cross-track (CT) direction and elevation direction, respectively. The ULA is fixed along the $y$-axis. When the platform moves forward, only one element is activated to transmit and receive the linear frequency modulated (LFM) signal during each pulse repetition time (PRT). These elements transmit signals sequentially with a high switching frequency.

Here we are to establish a 1D sparse model for LASAR. Because it is easy to obtain high resolutions in AT and elevation directions, we concentrate on the resolution improvement in CT direction only.

Since the resolution in CT direction is obtained by beamforming, it is convenient to use the polar coordinate in $yoz$ plane [1]. Thus, the scatter $\mathbf{P}(x_\mathbf{P}, y_\mathbf{P}, z_\mathbf{P})$ can also be expressed as $\mathbf{P}(x_\mathbf{P}, r_\mathbf{P}, \theta_\mathbf{P})$,

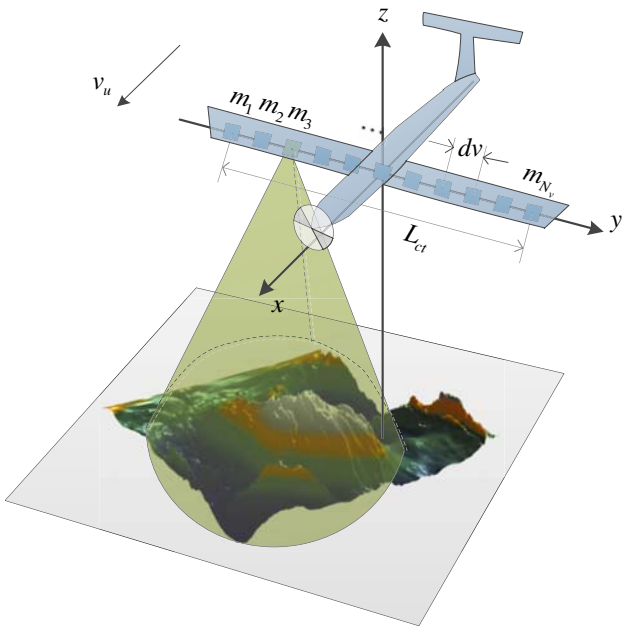


**Figure 1.** Geometrical model of 3D SAR with a ULA.

where $r_{\mathbf{P}} = \sqrt{(y_{\mathbf{P}})^2 + (z_{\mathbf{P}})^2}$ and $\theta = \arcsin(y_{\mathbf{P}}/r_{\mathbf{P}})$ (usually very small). When LASAR works under the downward-looking mode, its point spread function (PSF) [1, 23] can be formulated as:

$$\tilde{g}\left(x, r, \theta; \mathbf{P}\right) = \sigma_{\mathbf{P}} e^{j\psi(\mathbf{P})} \text{sinc}\left(\frac{x - x_{\mathbf{P}}}{\rho_x}\right) \text{sinc}\left(\frac{r - r_{\mathbf{P}}}{\rho_r}\right) \text{sinc}\left(\frac{\theta - \theta_{\mathbf{P}}}{\rho_\theta}\right) \tag{1}$$

where the sinc function is defined as $\text{sinc}(v) \triangleq \sin(\pi v)/\pi v$, and $\psi(\mathbf{P})$ is the residual phase of $\mathbf{P}$ after image focusing. $\rho_x$, $\rho_\theta$ and $\rho_r$ denote resolutions in AT, CT and range directions respectively.

The column image $g(x = x_i, r = r_k, \theta)$, for the $k$th equi-range slice and the $i$th column, can be expressed as:

$$g\left(x = x_i, r = r_k, \theta\right) = \sum_{\mathbf{P}} \mathbf{s}(\mathbf{P}) \text{sinc}\left(\frac{\theta - \theta_{\mathbf{P}}}{\rho_\theta}\right) + n_1(\theta) \tag{2}$$

where

$$\mathbf{s}(\mathbf{P}) = \sigma_{\mathbf{P}} e^{j\psi(\mathbf{P})} \text{sinc}\left(\frac{x_i - x_{\mathbf{P}}}{\rho_x}\right) \text{sinc}\left(\frac{r_k - r_{\mathbf{P}}}{\rho_r}\right) \tag{3}$$

$n_1(\theta)$ denotes the noise item. Further, formula (2) can be expressed as a linear system

$$\mathbf{g}_{(i,k)} = \mathbf{H}^\theta \mathbf{s}_{(i,k)} + \mathbf{n} \tag{4}$$

where $\mathbf{g}_{(i,k)}$ denotes the column image $g(x = x_i, r = r_k, \theta)$, $\mathbf{s}_{(i,k)}$ the sparse vector to be recovered, and $\mathbf{H}^\theta$ the measurement matrix, defined by

$$\mathbf{H}^\theta = \left[H_1^\theta, H_2^\theta, \cdots, H_q^\theta, \cdots, H_Q^\theta\right] \tag{5}$$

where $H_q^\theta = \text{sinc}(\boldsymbol{\theta} - \theta_q)$ denotes the $q$th column of $\mathbf{H}^\theta$, $\boldsymbol{\theta} = [0, d_\theta, \cdots, (Q-1)d_\theta]$, and $d_\theta$ is the pixel interval. How to determine the pixel interval $d_\theta$ will be discussed in Sections 2.3 and 4.

So far, we have obtained the 1-D sparse model of LASAR (4). Compared with the implementation in [20], the size of the measurement matrix has been reduced from $MQ \times MQ$ to $Q \times Q$ for the slice image of size $Q \times M$.

### 2.2. Recovery by $\ell_1$ Regularization

After establishing the sparse model of LASAR, we reformulate problem (4) as a series of $\ell_1$ regularization problems:

$$\hat{\mathbf{s}}_{(i,k)}^{\Re} = \min \|\mathbf{H}^{\theta}\mathbf{s}_{(i,k)}^{\Re} - \mathbf{g}_{(i,k)}^{\Re}\|_2^2 + \eta\|\mathbf{s}_{(i,k)}^{\Re}\|_1^1 \tag{6}$$

$$\hat{\mathbf{s}}_{(i,k)}^{\Im} = \min \|\mathbf{H}^{\theta}\mathbf{s}_{(i,k)}^{\Im} - \mathbf{g}_{(i,k)}^{\Im}\|_2^2 + \gamma\|\mathbf{s}_{(i,k)}^{\Im}\|_1^1 \tag{7}$$

where the superscripts $\Re$ and $\Im$ mean taking the real and imaginary parts, respectively. $\hat{\mathbf{s}}_{(i,k)}$ represents the estimate of $\mathbf{s}_{(i,k)}$. $\eta$ and $\gamma$ are the regularization parameters, and can be determined by the methods in [24]. Alternatively, in this paper, the least absolute selection and shrinkage operator (LASSO) [25], which does not require regularization parameters explicitly, is invoked to solve the problems (6) and (7).

Compared with [21], the proposed model can divide the complex-valued problem into the real and imaginary parts. It will not increase the size of the measurement matrix as in [21], thus this model can be suitable for larger scale problems.

### 2.3. The Pixel Interval and the Cross Coherence

Here we aim to find the influence of the pixel interval. It is important to note that we use SR to improve the resolution rather than to save the antenna elements [21], so we assume that the signals are full-sampled in CT direction. Define the cross coherence $\mu_c(\mathbf{H}^{\theta}, l)$ of $\mathbf{H}^{\theta}$ as:

$$\mu_c\left(\mathbf{H}^{\theta}, l\right) = \frac{\left\langle H_q^{\theta}, H_{q+l}^{\theta}\right\rangle}{\|H_q^{\theta}\|_2\|H_{q+l}^{\theta}\|_2} \tag{8}$$

where $l \in [-Q/2, \cdots, 0, \cdots, Q/2-1]$ represents the index interval between two columns. As a result, the mutual coherence $\mu(\mathbf{H}^{\theta})$ is the second largest value of $\mu_c(\mathbf{H}^{\theta}, l)$.

$$\mu\left(\mathbf{H}^{\theta}\right) = \max_{l\neq 0} |\mu_c(\mathbf{H}^{\theta}, l)| \tag{9}$$

**Property 1** *The cross coherence $\mu_c\left(\boldsymbol{H}^{\theta}, l\right)$ of $\boldsymbol{H}^{\theta}$, defined in (8), is a sinc function with respect to the interval $l$.*

*Proof:* Consider this problem in its continuous form, then (8) can be reformulated as

$$\mu_c\left(\mathbf{H}^{\theta}, l\right) = \frac{1}{\rho_{\theta}}\int \operatorname{sinc}\left(\frac{\theta}{\rho_{\theta}}\right)\operatorname{sinc}\left(\frac{\theta - l}{\rho_{\theta}}\right)d\theta \tag{10}$$

where $l$ is the continuous form of column interval. Owing to the convolution theorem, we obtain

$$\mu_c\left(\mathbf{H}^{\theta}, l\right) = \operatorname{sinc}\left(\frac{l}{\rho_{\theta}}\right) \tag{11}$$

If $d_{\theta} \to 0$, then $\mu(\mathbf{H}^{\theta}) \to 1$. Thus the mutual coherence is usually very high in RE. However, a larger mutual coherence leads to more difficulty in SR. *Property 1* indicates that $d_{\theta}$ should not be too small. In other words, the ability of resolution improvement is limited. According to Subsection 4.1, it is recommended that $d_{\theta}$ should better meet $1 \leq \frac{\rho_{\theta}}{d_{\theta}} \leq 5$.

Figure 2 draws the cross coherence $\mu_c(\mathbf{H}^{\theta}, l)$ with $Q = 1024$ and $\frac{\rho_{\theta}}{d_{\theta}} = 5$. It compares the cross coherence of $\mathbf{H}^{\theta}(\alpha = 22)$, $\mathbf{H}^{\theta}(\alpha = 3)$ and a Gaussian random matrix in uniform spherical ensemble (USE) [26], which is considered to have good performance in SR. It demonstrates that $\mathbf{H}^{\theta}$ usually has much higher mutual coherence in RE. That is why $\mathbf{H}^{\theta}$ performs worse than Gaussian random matrix in SR.

In order to improve the performance of $\mathbf{H}^{\theta}$, it had better reduce the mutual coherence. However, in RE, it is unable to reduce the mutual coherence for $|ld_{\theta}| \leq \rho_{\theta}$, such that we can concentrate only on the cross coherence reduction for $|ld_{\theta}| > \rho_{\theta}$, which can eliminate the influence from pixels $|ld_{\theta}| > \rho_{\theta}$ as much as possible. For this purpose, according to Equations (8) and (11), we propose to filter bases in $\mathbf{H}^{\theta}$ and column images by applying SVA (or adding windows).

## 3. FILTERING BASES BY SVA

Besides, the sidelobes of the *sinc* basis can be easily influenced by noise and interference, and they might cause the unstability of resolution enhancement. Thus, it is necessary to filter the bases of $\mathbf{H}^{\theta}$. In this section, SVA [22] is employed to suppress the *sinc* kernel. For the sake of simplicity, we use $g(m)$ to refer to the column image $g(x = x_i, r = r_k, \theta)$. Here, its Fourier data is $G(f)$ with a support region $-f_0 < f < f_0$, where $f_0$ represents half of the bandwidth, and $m$ indexes the image pixel.

SVA can be described as a frequency domain aperture function:

$$W(f) = a + 2w(m)\cos\left(2\pi\frac{f}{f_s}\right) \tag{12}$$

where $f_s$ denotes the sampling frequency. It imposes two constraints to $W(f)$, in order to obtain *unit gain* and *monotonic gain*:

$$a = 1 - 2w(m)\frac{\sin w_s}{w_s} \tag{13}$$

$$0 \le w(m) \le w_{\max} = \frac{w_s}{2[\sin w_s - w_s \cos w_s]} \tag{14}$$

where $w_s = 2\pi f_0/f_s$. Let the 1-D column image pass though the filter (12), then get

$$g'(m) = ag(m) + w(m)[g(m-1) + g(m+1)] \tag{15}$$

In fact, SVA attempts to find proper $a$ and $w(m)$ such that $|g'(m)|^2$ is minimized. Generally, it can be implemented through the following three steps:

**Step1.** Calculate $g'(m)$ for $w(m) = 0$ ($g_1(m)$) and $w_{\max}$ ($g_2(m)$) by (15);

**Step2.** If $g_1(m) \times g_2(m) < 0$, the output $g'(m) = 0$;

**Step3.** Otherwise, the output pixel is the $g'(m)$ with the lowest magnitude, that is, $g'(m) = \{|g'(m)| = \min\{|g_1(m)|, |g_2(m)|\}\}$.

SVA can suppress sidelobes of the *sinc* kernel without widening the mainlobe [22]. Therefore, it is reasonable to assume that each column of $\mathbf{H}^{\theta}$ keeps only the mainlobe of the *sinc* kernel after applying SVA, that is

$$H_p^{\theta} = \mathrm{sinc}(\boldsymbol{\theta} - \theta_p) \circ \left(|\boldsymbol{\theta} - \theta_p| < \alpha\frac{\rho_\theta}{2}\right) \tag{16}$$

where the symbol $\circ$ denotes the elementwise product, and $\alpha \in [2, 4]$, whereas $\alpha = 22$ is used for the situation without SVA.

Figure 2 shows that though the cross coherence $\mu_c(\mathbf{H}^{\theta}, l)$ within $|ld_\theta| \le 1.5\rho_\theta$ is still large, the cross coherence for $|ld_\theta| > 1.5\rho_\theta$ has been greatly reduced by filtering bases of $\mathbf{H}^{\theta}$. Therefore, it is promising to improve the performance of $\mathbf{H}^{\theta}$ in RE. This will be validated by numerical simulations in Section 4. The steps of the proposed RE algorithm are summarized in Algorithm 1.

## 4. NUMERICAL EXPERIMENT

In this section, plenty of experiments are designed to examine the proposed method and find out how many times the resolution can be improved in CT direction.

### 4.1. Resolution Enhancement Ability

Because SRAs are usually nonlinear methods, the traditional resolution definition for SAR is not suitable for RE by SRAs. In RE, the resolution depends on the pixel interval $d_\theta$. In order to find out how many times the resolution can be improved by SRAs, we propose the resolution enhancement ability (REA) $\kappa(\rho_\theta)$ which is defined as

$$\kappa(\rho_\theta) = \max_{d_\theta} \frac{\rho_\theta}{d_\theta} \; s.t. \; \frac{\|\hat{\mathbf{s}}_p - \mathbf{s}_p\|_2}{\|\mathbf{s}_p\|_2} \le \epsilon \text{ and } \forall p \le \frac{\rho_\theta}{d_\theta} \tag{17}$$

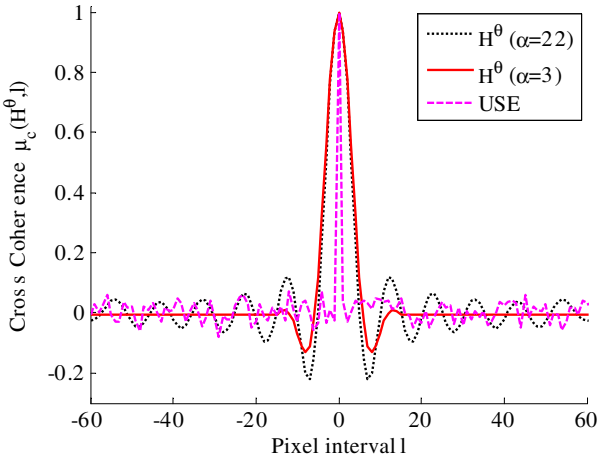


**Figure 2.** Cross coherence of measurement matrix.

**Algorithm 1** The resolution enhancement algorithm for LASAR

**Require:** LASAR echo data, radar parameters, *maxNSlice* {*maxNSlice denotes the max number of equi-range slices*}

1: Determine $\rho_\theta$, $d_\theta$, $M$, $Q$

**Ensure:** $1 \leq \frac{\rho_\theta}{d_\theta} \leq 5$

2: Use the polar coordinate in *yoz* plane and focus echo data by back projection (BP) algorithm

3: Build $\mathbf{H}^\theta$ and apply SVA to bases of $\mathbf{H}^\theta$

4: **for** $k = 1$: *maxNSlice* **do**

5: $\mathbf{G} \leftarrow k$th elevation slice image

6: Set the values for $\eta$ and $\gamma$

7: **for** $i = 1 : M$ **do**

8: Apply SVA to $G_i$, $\mathbf{g}_{(i,k)} \leftarrow G_i$

9: $\mathbf{g}^{\Re}_{(i,k)}$, $\mathbf{g}^{\Im}_{(i,k)}$

10: $\hat{\mathbf{s}}_{(i,k)} \leftarrow$ *sparse estimation by (6) and (7)*

11: **end for**

12: **end for**

where $\mathbf{s}_p$ denotes any $p$-sparse signal, and $\hat{\mathbf{s}}_p$ is the corresponding sparse recovery. $\epsilon$ is the acceptable relative $\ell_2$ norm error (RL2E). It implies that any $\mathbf{s}_p$ with $p \leq \kappa(\rho_\theta)$ should be recovered with the RL2E within $\epsilon$.

We designed several Monte Carlo experiments to find the approximate REA of $\mathbf{H}^\theta$ under different noise situations: SNR = 50 dB and SNR = 30 dB. In these experiments, the parameter $\alpha$ in (16) was selected as $\alpha_0 = 22$ for the situation without SVA and $\alpha_1 = 3$ for the situation with SVA. Let $d_\theta = 1$ and $Q = (10 + \alpha_0)\lceil \frac{\rho_\theta}{d_\theta} \rceil$. The sparsity $p$ varied from 1 to $\lfloor \frac{\rho_\theta}{d_\theta} \rfloor$, and all $p$ entries were randomly located but fell into the same resolution cell. For each different $\rho_\theta$, $\alpha$ and SNR, we carried out 200 Monte Carlo simulations to calculate the average RL2E. The simulation results are summarized in Figure 3.

In noise situations, we set $\epsilon = 0.1$. From Figure 3(a) (SNR = 50 dB), it is clear that $\rho_\theta = 4$ satisfies RL2Es $\leq \epsilon$ for $p \leq 4$, but the RL2E for $\rho_\theta = 5$ is more than $\epsilon$ when $p = 5$. Meanwhile, the $(\rho_\theta = 10, \alpha = 3)$ and $(\rho_\theta = 9, \alpha = 3)$ situations show much less RL2Es than those for $\alpha = 22$. Therefore, a conclusion is drawn that when SNR = 50 dB, the REA is about 4 for the situation without SVA; if SVA is applied, the REA can reach to about 9.

Figure 3(b) shows the RL2E curves when SNR = 30 dB. It is obvious that the noise degrades the performance of the measurement matrix. At this moment, the REA for the situation without SVA is

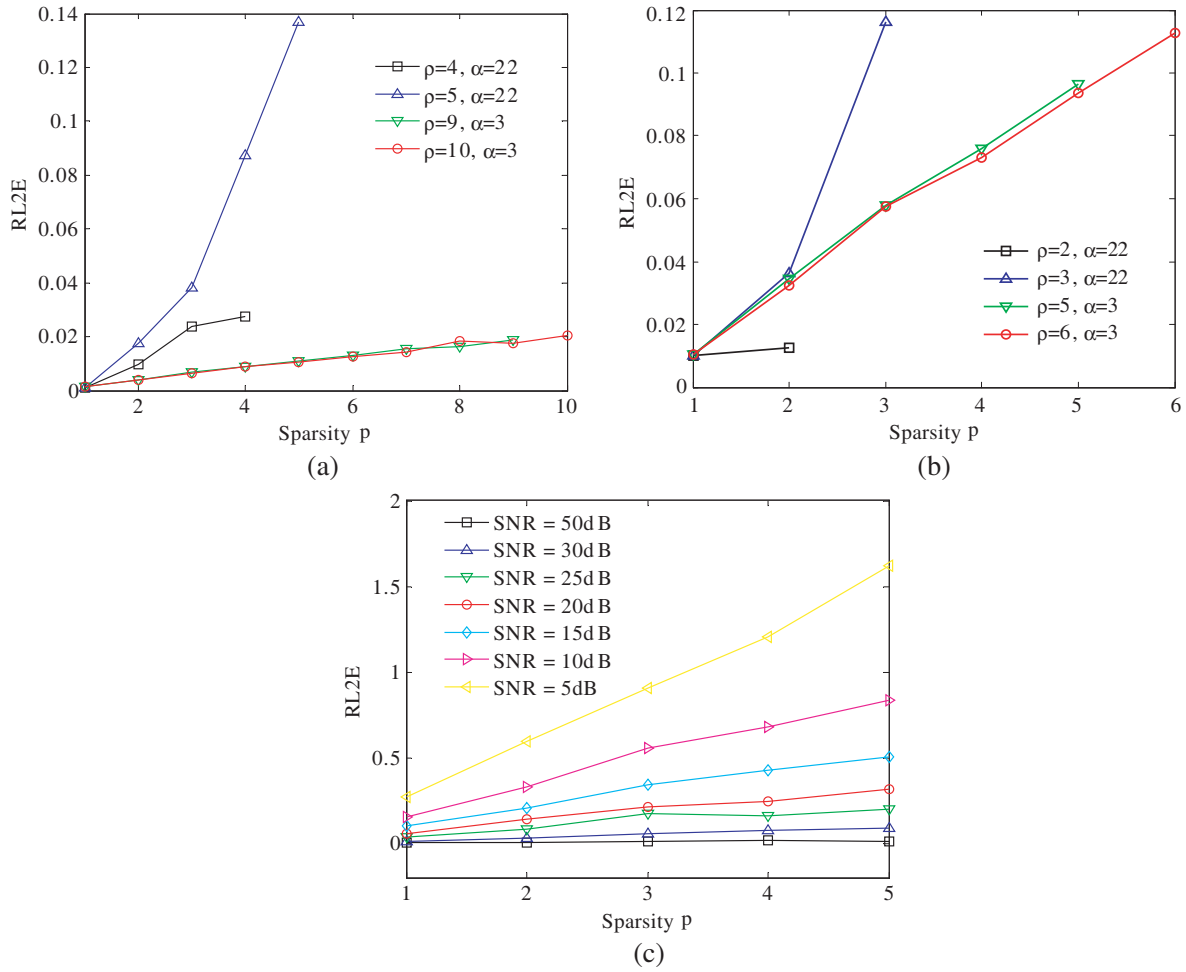


**Figure 3.** The results of Monte Carlo experiments: (a) the RL2E curves for SNR = 50 dB, (b) the RL2E curves for SNR = 30 dB, (c) the RL2E curves with respect to different SNRs with $\rho_\theta = 5$ and $\alpha = 3$.

about 2, but when SVA is applied, the REA is about 5. It is indicated that when SNR = 30 dB, the resolution can be improved only about 2 times without SVA, but if SVA is employed, the resolution can be improved by about 5 times. Thus, we suggest $1 \leq \frac{\rho_\theta}{d_\theta} \leq 5$.

To find the influence of SNR, we chose 7 different SNRs to perform Monte Carlo experiments with $\rho_\theta = 5$ and $\alpha = 3$. The RL2E curves corresponding to these SNRs are gathered in Figure 3(c). It is obvious that the higher SNR is, the better RL2E is obtained. We also find that only when SNR is better than about 30 dB, the proposed method performs well. This is because sparse reconstruction methods are usually noise sensitive, especially when the measurement matrix has a high mutual coherence. However, it is important to know that the resolution enhancement in CT direction is applied to a 3D focused data, which are acquired by 3D match filtering. Therefore, it is possible that the data in CT direction have a high SNR around 30 dB.

### 4.2. 3D Surface Terrain Simulation

In this subsection, we simulate a 3D surface terrain with flat tops to examine our sparse model for LASAR and to exhibit the ability of resolution enhancement. The original DEM data are shown in Figure 4(a), and the scatters are assumed to have equal amplitudes but uniform random phases. Assume the resolution $\rho_\theta = 0.01$(rad), the pixel interval $d_\theta = 0.002$(rad) and SNR = 30 dB. The measurement matrix $\mathbf{H}^\theta$ is the size of $256 \times 256$. According to Figure 4, it is obvious that the DEM of BP recovery

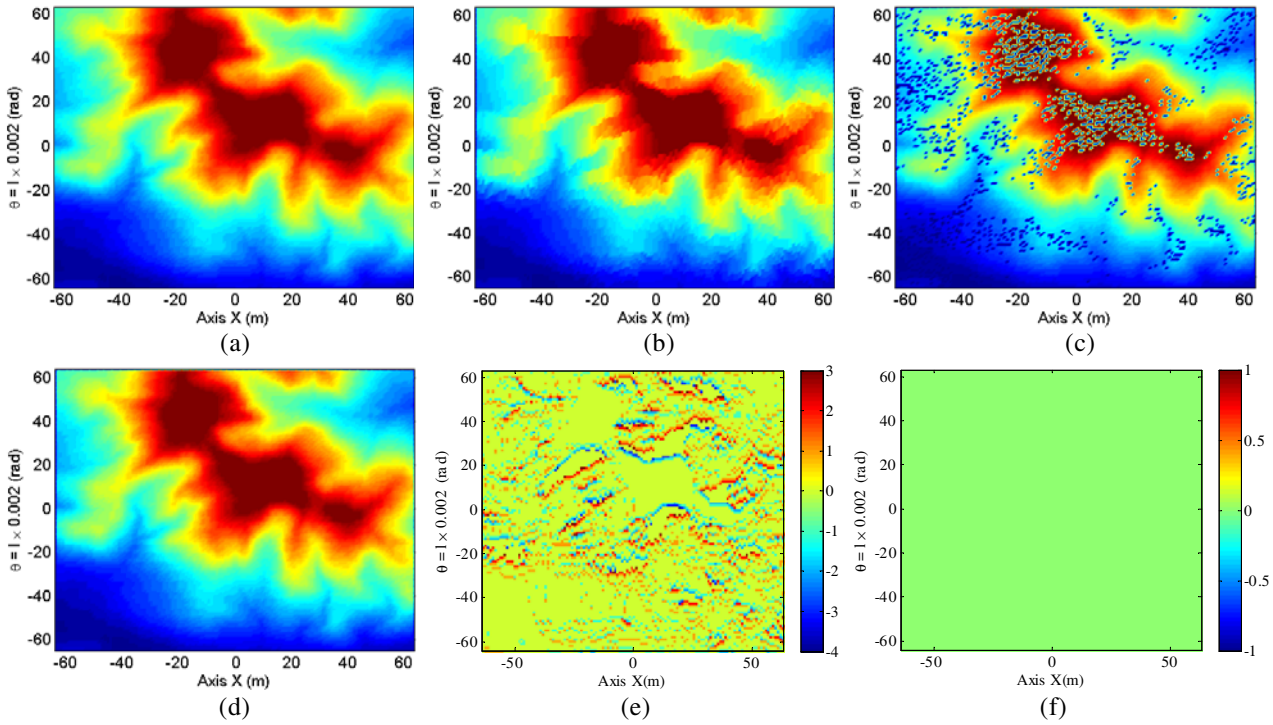


**Figure 4.** Resolution enhancement results for the 3D surface terrain with $\rho_\theta = 0.01$, $d_\theta = 0.002$: (a) The original DEM, (b) the DEM of BP recovery (clipped), (c) the DEM of sparse recovery (clipped, without SVA $\alpha = 22$), (d) the DEM of sparse recovery (clipped, with SVA $\alpha = 3$), (e) the residual error of DEM for BP recovery, (f) the residual error of DEM for sparse recovery (with SVA).

(see Figure 4(b)) shows lower resolution in CT direction; however, the DEM of sparse recovery with SVA (see Figure 4(d)) is very similar to the original DEM. The recovery errors shown in Figure 4(e) and Figure 4(f) also prove that our proposed method provides a more accurate reconstruction. However, in Figure 4(c), lots of pixels are not recovered correctly when SVA is absent. Therefore, it implies that the filtering bases of $\mathbf{H}^\theta$ can improve the performance of $\mathbf{H}^\theta$ in RE.

## 5. SUMMARY

In this paper, we focus on the resolution enhancement of LASAR and present a 1D sparse model for LASAR, which handles the 3D image column by column along CT direction in each equi-range slice. As a result, it greatly reduces the size of resolution enhancement problems, and it is suitable for large problems. In addition, for LASAR, its cross coherence is proven to be a *sinc* function in theory. Thus, the mutual coherence in resolution enhancement can be very high, such that the performance of SRAs will be greatly degraded. For a better performance, we propose to filter bases of the measurement matrix and the column images. The experimental results validate that when SNR = 30 dB, LASAR can usually obtain 2 times of resolution improvement in CT direction. Meanwhile, the filtering bases operation can further improve the REA by about 2.5 times, and the 3D surface terrain simulation shows a great improvement for the DEM reconstruction by our method. Besides, the proposed method can be applied to other situations with *sinc* kernel.

## ACKNOWLEDGMENT

This work was supported by the National Natural Science Foundation of China under Grant (No. 61101170) and the Ph.D. Programs Foundation of Ministry of Education of China

(No. 2011018511001). We would also like to thank the 701-4 lab of the University of Electronic Science and Technology of China (UESTC) for their challenging conversation and comments.

## REFERENCES

1. Klare, J., A. Brenner, and J. Ender, "A new airborne radar for 3D imaging — image formation using the ARTINO principle," *EUSAR*, Dresden, Germany, 2006.
2. Marechal, N., "Tomographic formulation of interferometric SAR for terrain elevation mapping," *IEEE Transactions on Geoscience and Remote Sensing*, Vol. 33, No. 3, 726–739, 1995.
3. Eineder, M., N. Adam, R. Bamler, et al., "Spaceborne spotlight SAR interferometry with TerraSAR-X," *IEEE Transactions on Geoscience and Remote Sensing*, Vol. 47, No. 5, 1524–1535, 2009.
4. Mahafza, B. R. and M. Sajjadi, "Three-dimensional SAR imaging using linear array in transverse motion," *IEEE Transactions on Aerospace and Electronic Systems*, Vol. 32, No. 1, 499–510, 1996.
5. Chan, T.-K., Y. Kuga, and A. Ishimaru, "Experimental studies on circular SAR imaging in clutter using angular correlation function technique," *IEEE Transactions on Geoscience and Remote Sensing*, Vol. 37, No. 5, 2192–2197, 1999.
6. Axelsson, S. R. J., "Mapping performance of curved-path SAR," *IEEE Transactions on Geoscience and Remote Sensing*, Vol. 40, No. 10, 2224–2228, 2002.
7. Axelsson, S. R. J., "Beam characteristics of three-dimensional SAR in curved or random paths," *IEEE Transactions on Geoscience and Remote Sensing*, Vol. 42, No. 10, 2324–2334, 2004.
8. Ishimaru, A., T.-K. Chan, and Y. Kuga, "An imaging technique using confocal circular synthetic aperture radar," *IEEE Transactions on Geoscience and Remote Sensing*, Vol. 36, No. 5, 1524–1530, 1998.
9. Weib, M. and J. H. G. Ender, "A 3D imaging radar for small unmanned airplanes — ARTINO," *European Radar Conference (EURAD)*, 209–212, 2005.
10. Shi, J., X. L. Zhang, J. Y. Yang, et al., "Experiment results on one-active LASAR," *IEEE Radar Conference*, 1–4, Pasadena, CA, 2009.
11. Xiang, G., X. L. Zhang, and J. Shi, "Airborne 3-D forward looking SAR imaging via chirp scaling algorithm," *IEEE International Geoscience and Remote Sensing Symposium (IGARSS)*, 3011–3014, 2011.
12. Ren, X. Z., J. T. Sun, and R. L. Yang, "A new three-dimensional imaging algorithm for airborne forward-looking SAR," *IEEE Geoscience and Remote Sensing Letters*, Vol. 8, No. 1, 153–157, 2011.
13. López-Dekker, P. and J. J. Mallorquí, "Capon- and APES- based SAR processing: Performance and practical considerations," *IEEE Transactions on Geoscience and Remote Sensing*, Vol. 48, No. 5, 2388–2402, 2010.
14. Xu, X. J. and R. M. Narayanan, "Enhanced resolution in SAR/ISAR imaging using iterative sidelobe apodization," *IEEE Transactions on Image Processing*, Vol. 14, No. 4, 537–547, 2005.
15. Lim, B. G., J. C. Woo, and Y. S. Kim, "Noniterative super-resolution technique combining SVA with modified geometric mean filter," *IEEE Geoscience and Remote Sensing Letters*, Vol. 7, No. 4, 713–717, 2010.
16. Bruckstein, A., D. Donoho, and M. Elad, "From sparse solutions of systems of equations to sparse modeling of signals and images," *Siam Review*, Vol. 51, No. 1, 34–81, 2009.
17. Potter, L. C., E. Ertin, J. T. Parker, et al., "Sparsity and compressed sensing in radar imaging," *Proceedings of the IEEE*, Vol. 98, No. 6, 1006–1020, 2010.
18. Zhu, X. X. and R. Bamler, "Super-resolution power and robustness of compressive sensing for spectral estimation with application to spaceborne tomographic SAR," *IEEE Transactions on Geoscience and Remote Sensing*, Vol. 50, No. 1, 247–258, 2012.
19. Wei, S. J. and X. L. Zhang, "Linear array SAR imaging via compressed sensing," *Progress In Electromagnetics Research*, Vol. 117, 299–319, 2011.

20. Shi, J., X. L. Zhang, G. Xiang, et al., "Signal processing for microwave array imaging: TDC and sparse recovery," *IEEE Transactions on Geoscience and Remote Sensing*, Vol. 50, No. 11, 4584–4598, 2012.
21. Wei, S. J. and X. L. Zhang, "Linear array SAR 3-D imaging based on compressed sensing," *Journal of Astronautics*, Vol. 32, No. 11, 2403–2409, 2011.
22. Smith, B. H., "Generalization of spatially variant apodization to noninteger Nyquist sampling rates," *IEEE Transactions on Image Processing*, Vol. 9, No. 6, 1088–1093, 2000.
23. Shi, J., X. L. Zhang, J. Y. Yang, et al., "Radix-N resolution-fusion for LASAR via orthogonal complement decomposition," *IEEE Geoscience and Remote Sensing Letters*, Vol. 6, No. 1, 147–151, 2009.
24. Batu, O. and M. Cetin, "Parameter selection in sparsity-driven SAR imaging," *IEEE Transactions on Aerospace and Electronic Systems*, Vol. 47, No. 4, 3040–3050, 2011.
25. Stodden, V., L. Carlin, D. Donoho, et al., "SparseLab," URL http://sparselab.stanford.edu/, 2013.
26. Tsaig, Y. and D. L. Donoho, "Extensions of compressed sensing," *Signal Processing*, Vol. 86, No. 3, 549–571, 2006.